FREELY CONVECTIVE MASS TRANSPORT IN A STRATIFIED FLUID

E. N. Korchagina and Yu. A. Sokovishin

UDC 536.252:66.015.23

Experimental and computed results are presented for the freely convective mass transport from a vertical salt surface in a stratified medium.

When salt is extracted underground through drill holes in a salt stratum, a chamber is formed whose size and shape are determined by the technological features of the solvent delivery. A vertical concentration gradient is formed in the reservoir. Experiments show that wall dissolution occurs under free convection conditions for a relationship $D_k/D_d > 0.12$ between the running and design diameters.

There are no data in the literature on freely convective mass transport in a stratified medium. However, the mass transport is modeled by heat transfer processes. Freely convective heat transfer is investigated analytically in a stratified medium for a power-law change in the temperature of the walls and the environment [1-3]. The greatest quantity of experimental and computed data is available on the heat elimination of a constant-temperature vertical surface for a linearly decreasing fluid temperature for Pr = 2-15 [2, 4, 5].

We examine the results of an experimental investigation and an approximate computation of the local mass transport from a rock salt surface for a different stratification of the brine. A transparent reservoir in the form of a parallelepiped (30 × 23 × 8 cm) fabricated from organic glass was the model of the underground chamber element. It was a sector equal to one-half a circular cylinder taken as the initial shape of the chamber. The front and its parallel model wall were equipped with a system of samplers arranged at the following spacings from the upper face: x = 1, 3, 5, 7, 9, 11, 14, 17 cm, and from the water delivery column: y = 6.5 and 10 cm.

The model was sealed by a lid with a rubber gasket and screws. The solvent delivery and brine sampling were executed by a system of pipe within a pipe. The brine was sampled over the inner column of diam. 1.2 mm, and the water entered the space between the pipes (inner diameter of the water delivery column was 6 mm). The brine intake column was in the lower part of the chamber, and the water delivery section was varied depending on the salt checkout technology. Solvent consumption was determined by a volume method by the rate of filling the measuring vessel at the exit from the chamber. One of the chamber walls was modeled by a transparent NaCl crystal, which permitted observation of the hydrodynamic flow pattern during dissolution. The flow was visualized by using dyes (acid chrome-dark-blue and methylthymol blue), for whose initiation in the water-delivery column a special branch pipe is provided. To visualize the zones of significant brine densities, tracing sheets with parallel oblique lines superposed by ink were fastened to the opposite side. To study the mass transfer under stratification conditions, the rock salt specimens were mounted in a sealed chamber with a flap.

M. P. Bel'dy (see [6]) proposed the method of determining the local rates of dissolution of different salts. The working surface is one of the faces of the salt specimen, 24 × 8 cm in size, in the vertical position. The checking tablets, fabricated by pressing salt powder to a density of $\rho = 2160$ kg/m^3, were mounted in a hole along the center line of the surface to be dissolved at the following distances from the upper face: Test No. 1, x = 1, 4, 7, 10, 14; Test No. 2, x = 2, 5, 8, 11, 14 cm. Upon the production of a definite stratification in the model, the flap was raised and the specimen was dissolved for 15 min. The change in weight of the control tablets, which was determined to ± 0.1 mg accuracy, permitted the determination of the local rate of salt dissolution.

The relationship between the geometric parameters of the chamber model under consideration and the productivity of the solvent can be found by using similarity theory. When modeling the underground dissolution process, two criteria, Fr/Re^2 = idem and Sc = idem, must be conserved.

All-Union Scientific-Research and Design Institute of Halurgy, Leningrad. Translated from Inzhenerno-Fizicheskii Zhurnal, Vol. 40, No. 3, pp. 440-446, March, 1981. Original article submitted March 4, 1980.

0022-0841/81/4003-0270$07.50

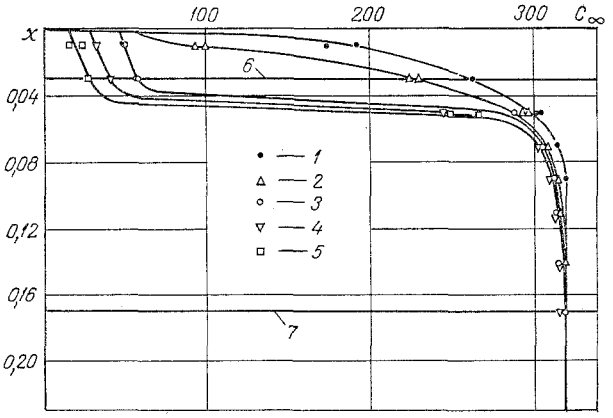

Fig. 1. Brine concentration distribution over the model height in Test No. 1 ($Q_m = 7.5 \cdot 10^{-8}$ m^3/sec, $C_{ini} = 0$): 1) $\tau = 4$ h; 2) 6; 3) 9; 4) 10; 5) $\tau = 11.5$ h; 6) water delivery level; 7) brine intake level; x, m; C_∞, kg/m^3.

The second condition is satisfied by selecting an identical physical medium for the modeling. It follows from the first condition that the productivity of the solvent delivered to the model is determined by the formula $Q_m = Q_n R_m H_m / (R_n H_n)$. The model productivity should be $Q_m = 7.3 \cdot 10^{-8}$ m^3/sec when modeling a natural chamber with the parameters $Q_n = 0.02$ m^3/sec, $R_n = 50$ m, $H_n = 25$ m.

The sequence in performing the experiment is the following. The model is filled with saturated brine, sealed and the salt is started to be washed out with a productivity Q_m. After a definite time, a sample is taken. When the whole saturated brine is replaced by new brine, the washing out ceases, the flap is opened and the specimen is dissolved under the conditions of produced stratification.

Distilled water, delivered to the chamber with a productivity $Q_m = 7.5 \cdot 10^{-8}$ m^3/sec at a distance of 3 cm from the chamber ceiling, was the solvent in Test No. 1. The washing out was total in 12 h. The change in concentration in the model is represented in Fig. 1. Upon delivery of the solvent at the chamber ceiling, and sampling the brine at its bottom, a slow piston displacement of the initial brine occurs and its replacement by new brine. The concentration varies exponentially with height. Mixing of the solvent with the brine occurs in a zone above the level of the water delivery, which causes a linear change in the concentration. The concentration does not vary along the horizontals.

The rate of mass transfer for a given concentration is determined by the distribution of the concentration before the model stops operating (Fig. 1, curve 5). Let us extract two sections with a characteristic change in concentration:

zone above water delivery (zone A)

$$C_w - C_\infty = -4x + 298, \quad x = 0 - 3\,\text{cm}; \tag{1}$$

zone of direct displacement of the brine (zone B)

$$C_w - C_\infty = 1500 \exp(-0.804x), \quad x = 3 - 15\,\text{cm}. \tag{2}$$

These two zones were also observed visually. The colored solvent delivered to the chamber was mixed intensely in zone A, producing a uniform tint. A layer by layer downward displacement of the fluid along the vertical occurred below the water delivery layer, where the clear horizontal boundary between the colored and uncolored brine descended slowly at a velocity of $\sim 2.8 \cdot 10^{-5}$ m/sec.

Test No. 2 consisted of two stages. In the first stage the water delivery column was lowered 14 cm downward from the upper face, which permitted observation of the mixing pattern in zone A (Fig. 2). Even 1.5 h after the beginning of the washing out at a productivity of $Q_m = 1.42 \cdot 10^{-7}$ m^3/sec, the concentration distribution in zone A (Fig. 2, curve 2) was characterized by uniformity along both the horizontal and the vertical. At this stage the water was delivered at a height of 2 cm from the upper face. Brine with a concentration of $C = 100$ kg/m^3 was used as solvent. The domain A (Fig. 2, curves 3 and 4) turned out to be very small and the concentration field was formed under conditions of displacing the brine in the whole chamber. Before the halt the concentration distribution took on a linear nature

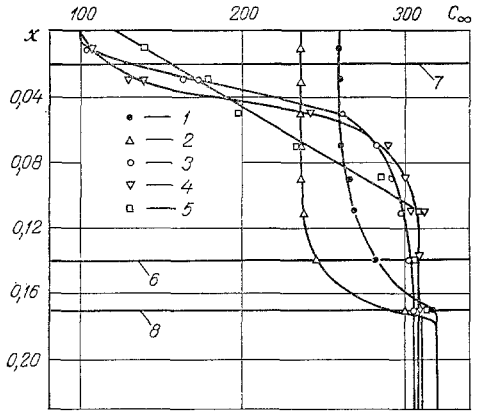

Fig. 2. Brine concentration distribution along the model height in Test No. 2: $Q_m = 1.42 \cdot 10^{-7}$ m^3/sec, $C_{ini} = 0$; 1) $\tau = 1$ h; 2) $\tau = 1.5$ h; 6) water supply level (first stage); $Q_m = 1.58 \cdot 10^{-7}$ m^3/sec; $C_{ini} = 100$ kg/m^3; 3) $\tau = 4$ h; 4) $\tau = 5.5$ h; 5) $\tau = 6$ h; 7) water supply level; 8) brine intake level (second stage).

$$C_w - C_\infty = 195.75 - 16.87x. \tag{3}$$

Dependences (1) and (2) for Test No. 1 and dependence (3) for Test No. 2 were initially used to study the NaCl specimen dissolution.

Experimental values of the local mass transfer characteristics are given in Table 1. Values of the weight ($\dot{m}_x$) and linear (W) dissolution rates are referred to the local brine concentration at this height. Comparing the data obtained with the results for a homogeneous concentration of the surrounding medium [7], the influence of stratification on the rate of salt surface dissolution can be explained. To obtain the computed values of the local dissolution rates we used an integral method [8].

The presence of the velocity maximum in a freely convective boundary layer permits separation of the boundary layer into two zones: inner ($y < y_m$) and outer ($y > y_m$).

The lift in the inner zone is in local equilibrium with the viscous forces, and the equation of motion has the form

$$\frac{\partial^2 u}{\partial y^2} = \frac{\rho - \rho_\infty}{\mu} g_x. \tag{4}$$

Since the lift is distributed between two domains, then the ratio

$$M = \frac{C_w - C_m}{C_w - C_\infty} = \frac{y_m}{\Delta_l} \tag{5}$$

characterizes that part concentrated in the inner zone. Assuming linearity of the concentration profile in the inner zone [9], we obtain

$$\rho - \rho_\infty = -\rho\beta (C_w - C_\infty)\left[1 - \frac{M}{y_m} y\right]. \tag{6}$$

Integrating (4) between $y = 0$ and $y = y_m$ with the boundary conditions $u = 0$ for $y = 0$ and $\partial u/\partial y = 0$ for $y = y_m$, we find the velocity distribution in the inner zone

$$u = \rho\beta \frac{C_w - C_\infty}{\mu} g_x \left[y y_m - \frac{y^2}{2} - M\left(\frac{y y_m}{2} - \frac{y^3}{6 y_m}\right)\right]. \tag{7}$$

Taking (7) into account, the total mass flow rate per unit width of surface will be

$$\Gamma_i = \frac{\rho^2 \beta (C_w - C_\infty)}{\mu} g_x \left(\frac{y_m^3}{3}\right)\left(1 - \frac{5M}{8}\right). \tag{8}$$

The total mass balance, written for the checking volume that includes the inner and outer domains is written as

$$D \frac{C_w - C_m}{y_m} = \frac{d}{dx}[\Gamma_i (\bar{C}_i - C_\infty)] + \frac{d}{dx}[\Gamma_0 (\bar{C}_0 - C_\infty)] + (\Gamma_0 + \Gamma_i)\frac{dC_\infty}{dx}. \tag{9}$$

TABLE 1. Comparison of Experimental and Theoretical Results on Salt Dissolution

x, m	C_∞, kg/m^2	Ra_x	$\dot{m}_{xp}$, kg/m^2·sec	w_e, m/sec	$\dot{m}_{xt}$, kg/m^2·sec	w_t, m/sec
			Test № 1			
0,01	15	$4{,}6\cdot10^{8}$	$5{,}5\cdot10^{-3}$	$2{,}55\cdot10^{-6}$	$6{,}0\cdot10^{-3}$	$2{,}7\cdot10^{-6}$
0,04	60	$2{,}9\cdot10^{10}$	$4{,}2\cdot10^{-3}$	$1{,}94\cdot10^{-6}$	$4{,}3\cdot10^{-3}$	$1{,}99\cdot10^{-6}$
0,07	305	$1{,}6\cdot10^{11}$	$0{,}11\cdot10^{-3}$	$0{,}05\cdot10^{-6}$	$0{,}08\cdot10^{-3}$	$0{,}04\cdot10^{-6}$
0,10	316	$4{,}6\cdot10^{11}$	$0{,}022\cdot10^{-3}$	$0{,}01\cdot10^{-6}$	$0{,}012\cdot10^{-3}$	$0{,}006\cdot10^{-6}$
0,14	317	$1{,}3\cdot10^{12}$	$0{,}015\cdot10^{-3}$	$0{,}007\cdot10^{-6}$	$0{,}009\cdot10^{-3}$	$0{,}004\cdot10^{-6}$
			Test № 2			
0,02	152	$5{,}0\cdot10^{9}$	$1{,}9\cdot10^{-3}$	$0{,}86\cdot10^{-6}$	$1{,}6\cdot10^{-3}$	$0{,}74\cdot10^{-6}$
0,05	195	$4{,}6\cdot10^{10}$	$1{,}0\cdot10^{-3}$	$0{,}46\cdot10^{-6}$	$0{,}95\cdot10^{-3}$	$0{,}44\cdot10^{-6}$
0,08	242	$9{,}7\cdot10^{10}$	$0{,}6\cdot10^{-3}$	$0{,}28\cdot10^{-6}$	$0{,}5\cdot10^{-3}$	$0{,}23\cdot10^{-6}$
0,11	308	$2{,}9\cdot10^{10}$	$0{,}12\cdot10^{-3}$	$0{,}05\cdot10^{-6}$	$0{,}08\cdot10^{-3}$	$0{,}04\cdot10^{-6}$
0,14	303	$9{,}2\cdot10^{10}$	$0{,}07\cdot10^{-3}$	$0{,}03\cdot10^{-6}$	$0{,}03\cdot10^{-3}$	$0{,}014\cdot10^{-6}$

Under the condition of linearity of the concentration profile in the inner zone, $\overline{C}_i$ can be found from the expression

$$\frac{\overline{C}_i - C_\infty}{C_w - C_m} = \frac{1}{M} - \frac{\frac{5}{8} - \frac{2M}{5}}{1 - \frac{5M}{8}}. \tag{10}$$

Using the notation

$$\gamma = \frac{d\Gamma_0}{d\Gamma_i}, \tag{11}$$

Equation (9) can be represented in the form

$$D(C_w - C_m) = y_m[C_1 + C_2\gamma]\frac{d}{dx}[(C_w - C_\infty)\Gamma_i] + y_m(1+\gamma)\Gamma_i\frac{dC_\infty}{dx}, \tag{12}$$

where

$$C_1 = \frac{\overline{C}_i - C_\infty}{C_w - C_\infty};\quad C_2 = \frac{\overline{C}_0 - C_\infty}{C_w - C_\infty}.$$

Finding y_m from (8) and substituting it into (12), the expression for Γ_i can be obtained

$$\Gamma_i = \left[\frac{4DM}{3(C_1+C_2\gamma)}\right]^{3/4}\left[\frac{\rho^2 g_x\beta\left(1-\frac{5M}{8}\right)}{3\mu}\right]^{1/4}x^{3/4}F^{3/4}, \tag{13}$$

where

$$F(x) = \frac{1}{x}\frac{\int_0^x (C_w - C_\infty)^{5/3}Gdx}{(C_w - C_\infty)^{4/3}G}, \tag{14}$$

$$G = \exp\int_0^x \frac{4}{3}\frac{1+\gamma}{C_1+C_2\gamma}\frac{1}{C_w - C_\infty}\frac{dC_\infty}{dx}dx. \tag{15}$$

Substituting (13) into (8), we determine the value of the quantity y_m. The magnitude of the local Nusselt number and the magnitude of the local mass flux $\dot{m}_x$ from the dissolution surface will be the final result:

$$Nu_x = C_l\left(\frac{g_x\beta(C_w - C_\infty)x^3}{\nu D}\right)^{1/4}\frac{(C_w - C_\infty)^{1/12}}{F^{1/4}}, \tag{16}$$

$$\dot{m}_x = C_l D\left(\frac{g_x\beta}{\nu D}\right)^{1/4}(C_w - C_\infty)^{5/3}G^{1/4}\frac{1}{\left[\int_0^x (C_w - C_\infty)^{5/3}Gdx\right]^{1/4}}, \tag{17}$$

where

$$C_l = \frac{M}{\left[\frac{4M}{(C_1 + C_2\gamma)\left(1 - \frac{5M}{8}\right)}\right]^{1/4}}.$$

The constants C_l, C_1, and C_2 are parameters dependent on the velocity and temperature distribution profiles, which are functions of the Schmidt number Sc, $n = (1 + \gamma)/(C_1 + C_2\gamma) - 1$.

A dependence of C_l on the number Pr is proposed in [10]:

$$C_l = \frac{0.50}{\left[1 + \left(\frac{0.49}{\mathrm{Pr}}\right)^{9/16}\right]^{4/9}}. \quad (18)$$

In the present experiment $\mathrm{Sc} \approx 1000$, hence $C_l = 0.497$ is taken. Computations executed for different values of n exhibited satisfactory agreement with the experiment for n = 4. Experimental and computed values, using (17), for the local dissolution rates of the vertical NaCl surface are represented in Table 1 for different stratifications of the surrounding medium.

The large density gradient, being formed at a distance of around 5 cm from the upper face in Test No. 1, caused a disturbance of the boundary layer flow, whereupon flow separation from the dissolution surface occurred. This phenomenon can be observed visually by using dyes sent out along the surface. The presence of a strong density gradient, moreover, directed against the flow, can be explained by the fact that experimental values greatly exceed the theoretical values for values of $x > 5$ in Test No. 1. For values of x in the mixing zone with a small density gradient, agreement between theory and experiment can be considered satisfactory.

Better agreement between the results of theory and experiment is observed in Test No. 2 with the linear brine density gradient over the height. An increase in the discrepancy of the data with distance from the upper face is also explained by disturbance of the laminarity of the flow caused by the density gradient directed opposite to the flow.

Therefore, for underground chambers of dissolution with a uniform brine density gradient over the height, the computation of the local mass transfer characteristics can be performed by means of (16) and (17) with (15) and (18) taken into account and for the value of n = 4.

NOTATION

x, vertical and y the transverse coordinates; D_k, chamber diameter; D_d, design chamber diameter; H, chamber height; Q, productivity of solvent pumping; τ, washout time; u, velocity component in the x direction; y_m, distance from wall to maximum velocity; Δ_l, thickness of the diffusion boundary layer; g, acceleration of gravity; μ, coefficient of dynamic viscosity; ρ, brine density; C, brine concentration; β, coefficient of volume expansion; Γ, mass flow rate per unit width of surface; $\dot{m}$, weight dissolution rate; W, linear dissolution rate; D, coefficient of molecular diffusion; $\mathrm{Sc} = \nu/D$, Schmidt number; $\mathrm{Pr} = \nu a$, Prandtl number; $\mathrm{Re} = uH/\nu$, Reynolds number; $\mathrm{Fr} = u/gH$, Froude number; $\mathrm{Ra}_x = g\beta x^3 \Delta C/\nu D$, Rayleigh number. Subscripts: m, model; n, nature; i, inner boundary layer domain; 0, outer boundary layer domain; x, local value; w, wall value; ∞, far from plate surface; m, at point of maximum velocity.

LITERATURE CITED

1. R. Cheesewright, "Natural convection from a plane, vertical surface in nonisothermal surroundings," Int. J. Heat Mass Transfer, 10, No. 12, 1847-1859 (1967).
2. R. Eichorn, "Natural convection in a thermally stratified fluid," in: Progress in Heat Transfer, Vol. 2, Pergamon Press, New York (1969), pp. 41-53.
3. K. T. Yang, F. L. Novotny, and Y. S. Cheng, "Laminar free convection from a nonisothermal plate immersed in a temperature-stratified medium," Int. J. Heat Mass Transfer, 15, No. 5, 1097-1109 (1972).
4. C. C. Chen and R. Eichorn, "Natural convection from a vertical surface to a thermally stratified fluid," Trans. ASME, 98C, No. 3, 446-451 (1976).
5. G. D. Raithby and K. G. T. Hollands, "Heat transfer by natural convection between a vertical surface and a stably stratified fluid," Trans. ASME, 100C, No. 2, 378-381 (1978).

6. B. P. Glukhov, "Investigation of the structure of hydrodynamic streams in a chamber for underground dissolution of rock salt deposits," Tr. VNIIG, No. 55, 95 (1971).
7. P. A. Kulle, Development of Salt Deposits by Leaching [in Russian], Goskhimizdat, Moscow–Leningrad (1949).
8. G. D. Raithby and K. G. T. Hollands, "A general method of obtaining approximate solutions to laminar and turbulent free convection problems," in: Advances in Heat Transfer, Vol. 11, Academic Press, New York (1975), pp. 265-315.
9. R. Cheesewright, "Turbulent natural convection from a vertical plane surface," Trans. ASME, 90C, No. 1, 1-9 (1968).
10. G. D. Raithby, K. G. T. Hollands, and T. E. Unny, "Analysis of heat transfer by natural convection across vertical fluid layers," Trans. ASME, 99C, No. 2, 287-293 (1977).

EVALUATING THE STRUCTURAL CHANGE IN ADSORBED WATER IN DISPERSED SYSTEMS DURING THEIR HYDRATION BY THE METHOD OF INFRARED SPECTROSCOPY

P. P. Olodovskii

UDC 541.182

On the basis of an analysis of the vibration frequency of D_2O molecules adsorbed on different ionic forms of montmorillonite, a method is proposed for evaluating the change in the density of this water in different groups.

Infrared spectroscopy was used in [1] to detect the existence of two types of groups of molecules of combined water and to evaluate their stability during dehydration.

This article carries the study to a second stage, investigating the effect of exchange cations on the change in the frequencies and force constants of water molecules adsorbed on montmorillonite.

The equipment and procedure used to obtain the measurements were detailed in [1].

Figures 1 and 2 show the change in the infrared spectra of deuterated Al- and Fe-forms of montmorillonite in the cases of desorption in the regions 1200-1500, 2500-2700, and 3500-3700 cm^{-1}. Similar spectra for the natural form are presented in [1].

It is known that the region 1200-1300 cm^{-1} corresponds to deformational vibrations of D_2O molecules, while the 1400-1450 cm^{-1} region corresponds to deformational vibrations of HDO. Thus, analysis of the resulting spectra is most conveniently begun by calculating the frequencies of these vibrations.

As was shown in [1], the greatest degree of hydration of the natural form of montmorillonite corresponds to a broad range, with a maximum of 1300 cm^{-1}; in the region of valence vibrations, the maximums of the corresponding ranges are 2680, 2610, and 2523 cm^{-1}. A relatively narrow band at 1264 cm^{-1} is distinguished on the general contour of the deformational vibration band as desorption proceeds, but it disappears at a low moisture content.

On the basis of calculation of the deformational vibration frequencies of H_2O molecules, we showed that the most stable molecules during desorption are those which interact with the exchange cation and an oxygen atom on the surface of the mineral, or with two oxygen atoms on the mineral surface [1].

Taking the values of the force constants characteristic of weak hydrogen bonds [2], we used our calculated data to obtain the frequency of the deformational vibrations of a symmetrical group – 1206 cm^{-1}. This frequency was not observed in the experiments. Calculation of the frequency for an asymmetrical group at the same force constants yielded a value of 1250 cm^{-1}.

Central Scientific-Research Institute of the Comprehensive Utilization of Water Resources of the Ministry of Water Management of the USSR, Minsk. Translated from Inzhenerno-Fizicheskii Zhurnal, Vol. 40, No. 3, pp. 447-454, March, 1981. Original article submitted January 25, 1980.

0022-0841/81/4003-0275$07.50